

# Potential Predictability of the Spring Bloom in the Southern Ocean Sea Ice Zone

Benjamin Buchovecky<sup>1</sup>, Graeme A. MacGilchrist<sup>2,3,4</sup>, Mitchell Bushuk<sup>2</sup>, F. Alexander Haumann<sup>3,5,6</sup>, Thomas L. Frölicher<sup>7,8</sup>, Natacha Le Grix<sup>7,8</sup>, John Dunne<sup>2</sup>

<sup>1</sup>Department of Geosciences, Princeton University, Princeton, NJ, USA

<sup>2</sup>NOAA Geophysical Fluid Dynamics Laboratory, Princeton, NJ, USA

<sup>3</sup>Program in Atmospheric and Oceanic Sciences, Princeton University, Princeton, NJ, USA

<sup>4</sup>School of Earth and Environmental Sciences, University of St. Andrews, St. Andrews, U.K.

<sup>5</sup>Alfred Wegener Institute Helmholtz Centre for Polar and Marine Research, Bremerhaven, Germany

<sup>6</sup>Ludwig-Maximilian-University Munich, Munich, Germany

<sup>7</sup>Climate and Environmental Physics, Physics Institute, University of Bern, Bern, 3012, Switzerland

<sup>8</sup>Oeschger Centre for Climate Change Research, University of Bern, Bern, 3012, Switzerland

## Key Points:

- Southern Ocean net primary production (NPP) is potentially predictable seven to ten years in advance in a perfect model experiment
- The peak predictability of NPP in November lags the peak predictability of sea ice extent and net shortwave radiation by two to three months
- Seasonal progression of predictability suggests that sea ice and light limitation control the inherent predictability of the spring bloom

---

Corresponding author: Graeme MacGilchrist, [graeme.macgilchrist@gmail.com](mailto:graeme.macgilchrist@gmail.com)

## Abstract

Every austral spring when Antarctic sea ice melts, favorable growing conditions lead to an intense phytoplankton bloom, which supports much of the local marine ecosystem. Recent studies have found that Antarctic sea ice is predictable several years in advance, suggesting that the spring bloom might exhibit similar predictability. Using a suite of perfect model predictability experiments, we find that November net primary production (NPP) is potentially predictable seven to ten years in advance in many Southern Ocean regions. Sea ice extent predictability peaks in late winter, followed by absorbed shortwave radiation and NPP with a two to three months lag. This seasonal progression of predictability supports our hypothesis that sea ice and light limitation control the inherent predictability of the spring bloom. Our results suggest skillful interannual predictions of NPP may be achievable, with implications for managing fisheries and the marine ecosystem, and guiding conservation policy in the Southern Ocean.

## Plain Language Summary

In very much the same way as we do for the weather, we can make forecasts of many aspects of the earth system. For example, rather than trying to predict how much rain will fall next Tuesday, we can explore how much algal growth might take place in the oceans around Antarctica in several months time. Such predictions could be extremely useful for managing the fragile ecosystems of these regions, for example informing fishing quotas in an upcoming season. However, just like for weather forecasts, there are upper limits for how far into the future we can expect to accurately make such predictions. It's this upper limit that we try to understand in this theoretical modeling study. We find that the upper limit is actually rather long (as much as 10 years!), and show that this is because of the close relationship between algal growth and sea ice (ice formed at the ocean surface) in this cold polar region. In turn, the extent of the sea ice can be predicted a long time in advance because there is a lot "memory" in this component of the earth system.

## 1 Introduction

Marine ecosystems are sustained at their base by net primary production (NPP). Variations in NPP cascade upward to higher trophic levels, driving variations in living marine organisms (e.g., zooplankton, or krill), which are sensitive to changing environmental conditions (Chassot et al., 2010; Stock et al., 2014; Tagliabue et al., 2021). In the Southern Ocean's seasonal ice zone, where sea ice seasonally extends and retreats, phytoplankton grow intensely for a relatively short period (<10 weeks) during the austral spring, resulting in a rapid increase in NPP (Moore & Abbott, 2000; Arrigo et al., 2008; Uchida et al., 2019; Arteaga et al., 2020; Douglas et al., 2023). In the subpolar Southern Ocean, across both the seasonal ice zone and Antarctic coastal polynyas (a region that we collectively call the sea ice zone), the spring increase in NPP from intense phytoplankton growth accounts for as much as 15% of total annual NPP in the Southern Ocean (Arrigo et al., 2008; Taylor et al., 2013). These short annual periods of intense growth, or blooms, are thus an important driver of the Southern Ocean marine ecosystem. Even though the relationship between NPP and upper trophic level biomass is complex (Friedland et al., 2012; Stock et al., 2017), skillful predictions of monthly NPP on seasonal-to-interannual time scales that capture the fluctuations in spring bloom production may help to better constrain predictions of ecological quantities and assist stakeholders in fishery management and marine conservation (Deppeler & Davidson, 2017; Moreau et al., 2020; Brooks & Ainley, 2022).

The spring bloom is closely linked to the seasonal retreat of sea ice (Moore & Abbott, 2000; Arrigo et al., 2008; Uchida et al., 2019; Arteaga et al., 2020), which has been shown to be predictable. Perfect model (PM) experiments, which assess the "potential

71 predictability” of the climate state assuming perfectly known initial conditions and per-  
72 fectly known model physics, show that the Antarctic sea ice edge location has interan-  
73 nual predictability with lead times of up to three years (Holland et al., 2013; Marchi et  
74 al., 2019). Using suites of initialized hindcasts from a General Circulation Model (GCM),  
75 Bushuk et al. (2021) found that observed winter Antarctic sea ice extent can be skill-  
76 fully predicted with an 11-month lead in the Weddell, Amundsen/Bellingshausen, Indian,  
77 and West Pacific sectors. These PM experiments and GCM-based hindcasts attribute  
78 the predictability and prediction skill of Antarctic sea ice to the significant thermal in-  
79ertia of the ocean which causes ocean heat content anomalies to remain at depth over  
80 the summer and reemerge during the autumnal sea ice advance, while being transported  
81 by the mean ocean circulation (Holland et al., 2013; Marchi et al., 2019; Bushuk et al.,  
82 2021).

83 Over the past decade, the potential for skillful seasonal-to-interannual predictions  
84 of marine primary production has been shown (S  ferian et al., 2014; Park et al., 2019;  
85 Fr  licher et al., 2020). This work has revealed that skill exists in locations where the rate  
86 of phytoplankton growth is determined by a process that itself exhibits predictability,  
87 *e.g.* nutrient supply (Krumhardt et al., 2020; Ham et al., 2021; Brune et al., 2022). To  
88 date, no study has focused on the sea ice zone. Given the robust seasonal prediction skill  
89 of Antarctic sea ice extent and the importance of sea ice to the sea ice zone spring bloom,  
90 we ask the question: How predictable is spring bloom NPP in the Southern Ocean sea  
91 ice zone and what are the main drivers of spring bloom predictability?

92 In this study, we assess the regional potential predictability of spring bloom NPP  
93 in the Southern Ocean using a suite of PM experiments performed with an ESM. After  
94 finding that spring bloom NPP and its associated physical drivers are predictable on seasonal-  
95 to-interannual time scales, we use a lead/lag diagnostic correlation analysis to elucidate  
96 the mechanisms of NPP predictability in this model.

## 97 2 Methodology

98 Model simulations were performed with the Earth System Model ESM2M (Dunne  
99 et al., 2012, 2013) developed by the Geophysical Fluid Dynamics Laboratory (GFDL).  
100 The GFDL-ESM2M model is a fully-coupled ESM with atmosphere, land, ocean, and  
101 sea ice components, and includes interactive ocean biogeochemistry. The atmosphere com-  
102 ponent is nearly identical to that in the GFDL Climate Model 2.1 (Delworth et al., 2006)  
103 and has 24 vertical layers with a horizontal resolution of 2   latitude by 2.5   longitude.  
104 The ocean component uses the MOM4 model (Griffies et al., 2005) with 50 vertical lay-  
105 ers and a nominal horizontal grid resolution of 1   latitude by 1   longitude, refined smoothly  
106 to 1/3   resolution at the equator. The sea ice component uses the same grid as the ocean  
107 component and simulates three thermodynamic layers, five ice thickness categories, and  
108 elastic-viscous-plastic sea ice dynamics (Winton, 1999).

109 The GFDL-ESM2M model simulates ocean biogeochemistry using the Tracers of  
110 Ocean Phytoplankton with Allometric Zooplankton version 2.0 (TOPAZv2), which mod-  
111 els 30 tracers to describe cycles of carbon, nitrogen, phosphorus, silicon, iron, oxygen,  
112 alkalinity, lithogenic material, and surface sediment calcite (Dunne et al., 2013). TOPAZv2  
113 resolves three phytoplankton groups: small (cyanobacteria and picoeukaryotes), large  
114 (diatoms and other eukaryotes), and diazotrophs (nitrogen-fixing phytoplankton). The  
115 rate of phytoplankton growth depends on irradiance, nutrient availability, and temper-  
116 ature. Organic biomass is lost through grazing by zooplankton and direct bacterial res-  
117 piration. In this study, we consider NPP integrated over the top 100 m of the ocean, where  
118 the majority of phytoplankton growth takes place.

119 We use a preindustrial control simulation and a suite of PM experiments conducted  
120 with GFDL-ESM2M as described in Fr  licher et al. (2020). A 300-year preindustrial con-

121 trol simulation is branched from a 1000-year quasi-steady-state simulation initialized with  
 122 conditions from 1860 (Dunne et al., 2012). The PM experiments branch off from the prein-  
 123 dustrial control simulation at six different start dates: January 1<sup>st</sup> in the years 22, 64,  
 124 106, 170, 232, and 295 (years chosen at random). Each start date contains 40 ensemble  
 125 members, each initialized with an infinitesimal perturbation in SST added to a single  
 126 grid cell in the Weddell Sea. The perturbations applied to the ensemble members were  
 127 evenly distributed between 0.002 and  $-0.002^{\circ}\text{C}$ . Each ensemble member was forced with  
 128 identical preindustrial boundary conditions and was run for a duration of 10 years with  
 129 the last ensemble group extending beyond the preindustrial control simulation by five  
 130 years. The temporal resolution of all variables analyzed here is monthly mean.

131 We use the prognostic potential predictability (PPP) metric to assess the predictabil-  
 132 ity of NPP and quantities relevant to the spring bloom. The PPP is an estimate of the  
 133 inherent upper limit of prediction skill of a given model. From Pohlmann et al. (2004),  
 134 PPP is given by the following equation:

$$PPP(\tau) = 1 - \frac{\frac{1}{N(M-1)} \sum_{j=1}^N \sum_{i=1}^M (X_{ij}(\tau) - \bar{X}_j(\tau))^2}{\sigma_c^2}$$

135 where  $X_{ij}$  is the value of a given variable for the  $i$ th ensemble member of the  $j$ th ensem-  
 136 ble,  $\bar{X}_j$  is the  $j$ th ensemble mean,  $\sigma_c^2$  is the variance of the control simulation for a given  
 137 target month,  $N$  is the number of ensembles ( $N = 6$ ),  $M$  is the number of ensemble  
 138 members ( $M = 40$ ), and  $\tau$  is the forecast lead time. Intuitively, PPP assesses how en-  
 139 semble members chaotically diverge over time by comparing the ensemble spread to the  
 140 natural variability of the control simulation. When PPP is equal to zero, the ensemble  
 141 spread is identical to the simulated natural variability of the control simulation, which  
 142 indicates that the variable could not have been skillfully predicted from the initial con-  
 143 ditions. When PPP is equal to one, the spread of the ensemble members is perfectly dis-  
 144 tinguishable from the simulated natural variability which indicates that the model is ca-  
 145 pable of perfectly predicting the variable given accurate initial conditions.

146 For our diagnostic analysis, we compute the Pearson correlation coefficient between  
 147 NPP at a target month and a predictor variable at months leading the target month.  
 148 We perform this correlation analysis for all twelve target months with a maximum lead  
 149 time of 13 months. For both the PM predictability assessment and diagnostic correla-  
 150 tion analysis, we consider six sectors of the Southern Ocean in our study: Weddell ( $60^{\circ}\text{W}$ -  
 151  $20^{\circ}\text{E}$ ), Indian ( $20^{\circ}\text{E}$ - $90^{\circ}\text{E}$ ), West Pacific ( $90^{\circ}\text{E}$ - $160^{\circ}\text{E}$ ), Ross ( $160^{\circ}\text{E}$ - $130^{\circ}\text{W}$ ), and Amund-  
 152 sen and Bellingshausen ( $130^{\circ}\text{W}$ - $60^{\circ}\text{W}$ ), plus the pan-Antarctic region, which encompasses  
 153 all aforementioned sectors, following Bushuk et al. (2021). To capture the sea ice zone,  
 154 the northern boundary for all sectors is  $55^{\circ}\text{S}$  and the southern boundary is the Antarc-  
 155 tic continent. The sector boundaries are shown in Supporting Fig. S1, and seasonal cli-  
 156 matologies of relevant variables in each sector are shown in Supporting Fig. S2. We per-  
 157 form an  $F$ -test with the ensemble and control run variances to determine significant PPP  
 158 values above the 95% confidence level ( $PPP > 0.183$ ), and use a  $t$ -test that accounts for  
 159 autocorrelation following Bretherton et al. (1999) to determine significant correlation co-  
 160 efficients above the 95% confidence level.

### 161 3 Results

162 Fig. 1 shows PPP time series for NPP over the ten-year forecast period. Since the  
 163 suite of PM experiments are initialized on January 1<sup>st</sup>, near perfect NPP potential pre-  
 164 dictability ( $PPP > 0.9$ ) exists in January of the first year (Fig. 1; see bottom-left corner  
 165 of each panel). At longer forecast times, NPP potential predictability decreases as the  
 166 initial perturbations of the ensemble members grow chaotically and diverge, making it  
 167 more difficult to predict their future state from the initial conditions. Across all regions,  
 168 the highest PPP values occur in spring, from October to December, indicating that spring  
 169 NPP is potentially predictable. NPP in the Weddell sector (Fig. 1b) has the highest spring

170 PPP throughout the forecast period, maintaining predictability for NPP in September  
 171 through December beyond the 10 year lead times. The Indian (Fig. 1c) and West Pa-  
 172 cific sectors (Fig. 1d) have lower PPP than the Weddell sector, but PPP remains sig-  
 173 nificant in November for several years. NPP in the Amundsen/Bellingshausen sector (Fig. 1f)  
 174 has high PPP for up to ten years in the spring with maximum PPP in December. Un-  
 175 like the other sectors, Ross sector NPP does not have consistently significant PPP in the  
 176 spring (Fig. 1e). While we show that NPP is predictable on interannual time scales, the  
 177 highest PPP values ( $>0.4$ ) occur in November of the first forecast year, suggesting that  
 178 nearly half of the spring NPP variance can be predicted almost one year in advance. We  
 179 focus our further analysis on this first-year November maximum to elucidate the key drivers  
 180 of NPP predictability.

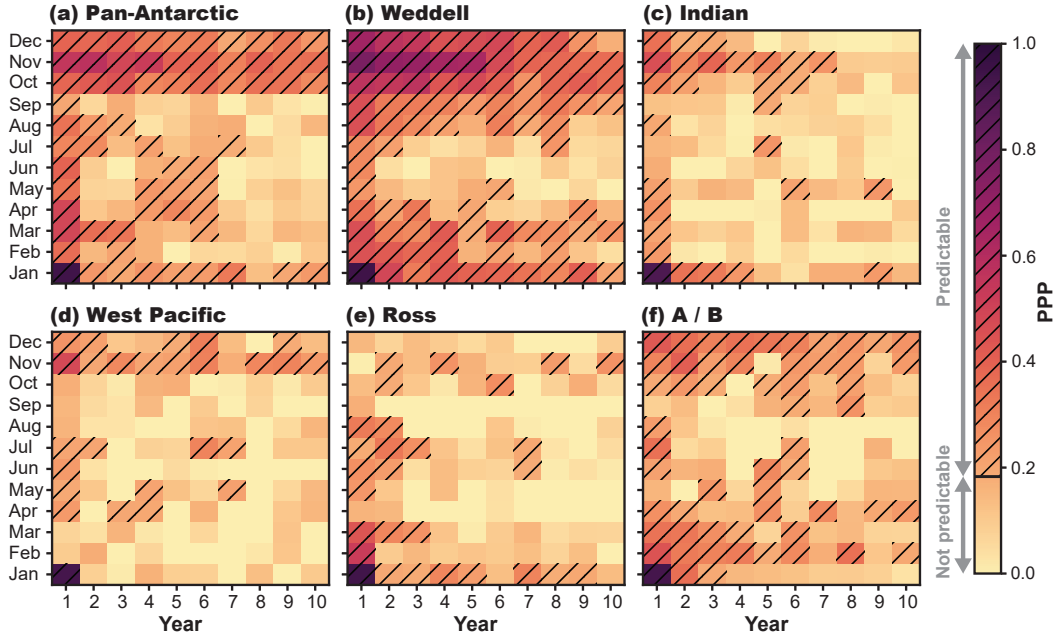


**Figure 1.** Regional predictability of net primary production (NPP) given by the prognostic potential predictability (PPP) metric computed from a suite of perfect model (PM) experiments with the GFDL-ESM2M model. The full ten-year forecast period from the PM ensembles is displayed with forecast years on the x-axis and months on the y-axis. PPP values above the 0.183 significance threshold are hatched and have a 95% confidence level based on an  $F$ -test.

181 Fig. 2 shows the regional predictability of NPP and potential key drivers of the sea  
 182 ice zone spring bloom (SIE, mixed-layer depth, surface irradiance, and surface dissolved  
 183 iron) for the first 13 months of the forecast period. As in Fig. 1, NPP predictability  
 184 peaks in November for the pan-Antarctic (Fig. 2a), Weddell (Fig. 2b), Indian (Fig. 2c), and  
 185 West Pacific (Fig. 2d) sectors while the Amundsen/Bellingshausen (A/B; Fig. 2f) sec-  
 186 tor has maximum NPP predictability in December. Spring NPP is generally unpredictable  
 187 in the Ross sector (Fig. 2e). In the Pan-Antarctic case, as well as prominently in the Wed-  
 188 dell, Indian, West Pacific, and A/B, the November peak in NPP predictability is pre-  
 189 ceded by — at one to two month leads — that of SIE and surface irradiance, indicat-  
 190 ing that the alleviation of light limitation could be a prominent source of NPP predictabil-  
 191 ity. Peaks in SIE predictability are accompanied, or slightly preceded, by peaks in MLD  
 192 predictability (in all except the West Pacific and Ross sectors) consistent with the link  
 193 between SIE predictability and the upward mixing of subsurface heat (Bushuk et al., 2021).  
 194 In the A/B and, to a lesser extent, Indian sectors, the timing of high surface iron pre-

195 dictability — which follows that of the MLD and precedes that of NPP — indicates that  
 196 alleviation of nutrient limitation could be an important source of NPP predictability in  
 197 that area. While wintertime iron predictability is high in other areas (specifically the Wed-  
 198 dell and Ross sectors), its alignment with spring bloom NPP predictability is less clear.  
 199 In the following, we highlight the potential role played by SIE and surface irradiance as  
 200 a source of NPP predictability, and revisit the role of iron in the discussion. The role of  
 201 temperature in mediating NPP and its predictability is addressed in Supporting Text  
 202 S1.

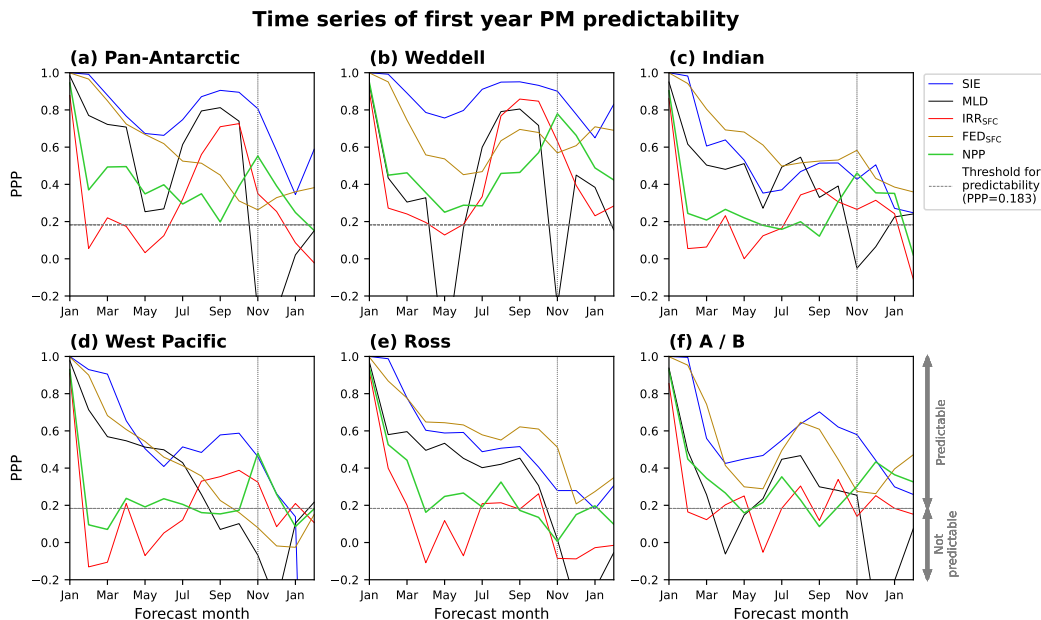


**Figure 2.** Regional predictability of sea ice extent (SIE), mixed layer depth (MLD), surface irradiance (IRR<sub>SFC</sub>), surface dissolved iron (FED<sub>SFC</sub>), and net primary production (NPP) determined by the PPP metric. The dotted vertical line marks November in the first forecast year. PPP values above 0.183 (horizontal dashed line) are significant at a 95% confidence level based on an  $F$ -test. PPP values above the significance threshold indicate that anomalies of the given variable are predictable with the ESM2M model given perfect initial conditions.

203 In Fig. 3, we arrange key spring bloom drivers and NPP according to the timing  
 204 of their respective peaks in predictability. We also add the PM predictability of surface  
 205 chlorophyll  $a$  (Chl  $a$ ) concentration and surface biomass since these metrics can be es-  
 206 timated using satellite (Behrenfeld et al., 2017) and biogeochemical float (Arteaga et al.,  
 207 2020) data, and could be integrated into operational forecasts informed by these PM pre-  
 208 dictability results. Aside from the Ross sector, all regions exhibit a diagonal structure  
 209 in their predictability peaks in Fig. 3, suggesting a progression of predictability start-  
 210 ing with SIE and MLD, followed by surface irradiance, and finally NPP. The pan-Antarctic  
 211 (Fig. 3a), Weddell (Fig. 3b), and Indian (Fig. 3c) sectors have the most defined progres-  
 212 sion of predictability with a two to three months lag between maximum SIE and NPP  
 213 predictability. In these regions, we also see maximum predictability for Chl  $a$  and sur-  
 214 face biomass lagging the November peak in NPP predictability by one to three months.  
 215 The West Pacific (Fig. 3d) and Amundsen/Bellingshausen (Fig. 3f) sectors display a less  
 216 defined diagonal structure but still exhibit a two to three months lag between maximum  
 217 SIE and NPP predictability. An equivalent perspective for the progression of predictabil-  
 218 ity from MLD, to surface iron, to NPP (Supporting Fig. S5) shows that while it may

219 be present in some sectors (specifically A/B, Weddell, and Indian), it is notably absent  
 220 in others, and for the Pan-Antarctic. In either case, these results support the interpretation  
 221 that the spring bloom mechanism (Fig. 3g, further discussed below) causes the  
 222 elevated predictability of spring NPP in the model simulations.

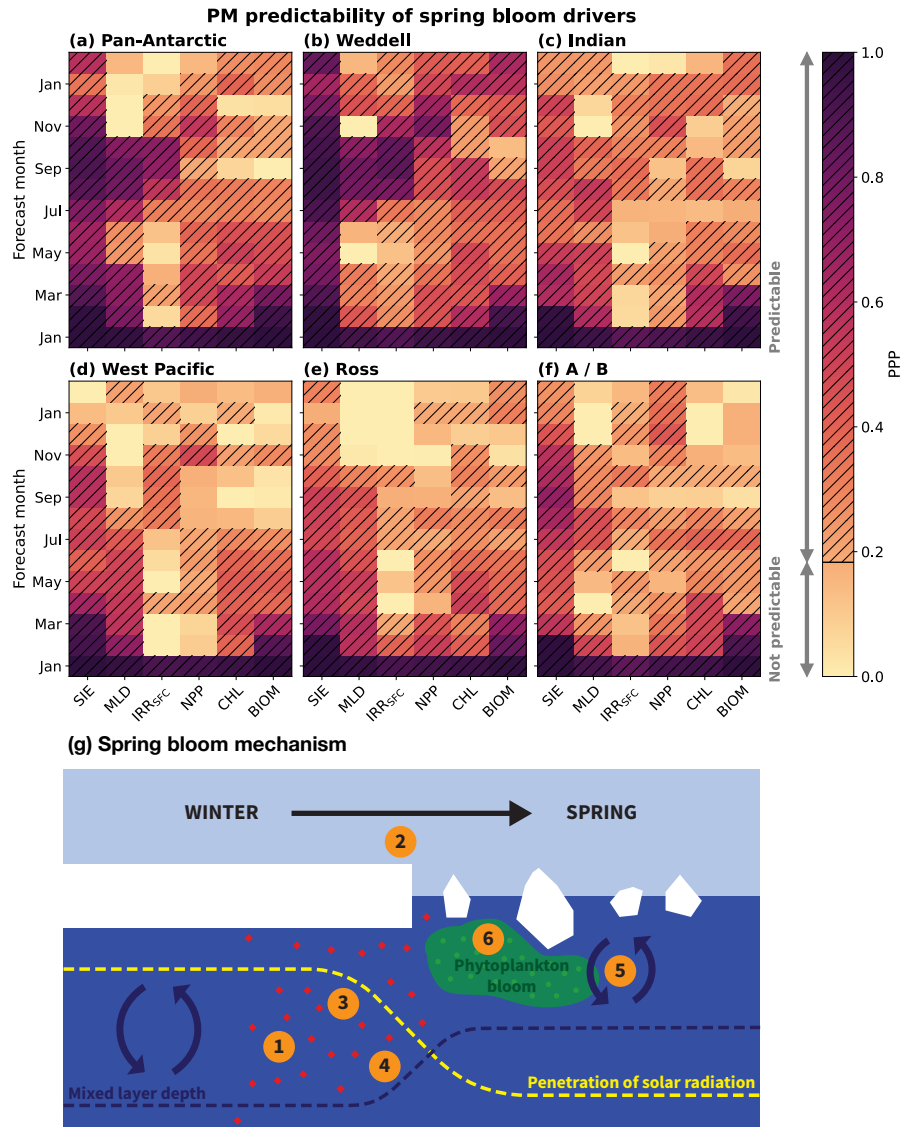


**Figure 3.** (a-f) Regional predictability of SIE, MLD, surface irradiance, NPP, Chl *a*, and surface biomass given by the PPP metric computed from a suite of PM experiments. Here, we display the first year of forecast time and arrange the variables on the x-axis following what we expect from the climatological spring bloom mechanism. (g) The mechanism of the climatological spring phytoplankton bloom. 1) Accumulation of nutrients in mixed layer during winter. 2) Sea ice melts and retreats. 3) Ocean surface receives more solar radiation, penetrates deeper into the water column. 4) The MLD shoals due to an influx of fresh melt water and greater solar radiation. 5) The shallow MLD traps phytoplankton and nutrients near the surface where light is abundant. 6) Phytoplankton grows intensely in the favorable conditions, forming the spring bloom.

223 To further examine the spring bloom and the relationship between its drivers and  
 224 NPP, we perform a correlation analysis of SIE and surface irradiance anomalies preced-  
 225 ing NPP anomalies up to 13 months in advance using the 300-year preindustrial control  
 226 simulation (Fig. 4). The colormap reveals the correlation of NPP in each target month  
 227 (displayed along the x-axis) with SIE (top) and  $IRR_{SFC}$  (bottom; positive downwards)  
 228 for each lead time (displayed along the y-axis). For example, the value at target month  
 229 November and lead three months provides the correlation between November NPP and  
 230 SIE/ $IRR_{SFC}$  in the previous August. Correlation values for NPP target months outside  
 231 September to March should be viewed cautiously due to the low absolute magnitude and  
 232 variance of NPP during those months. Consistent with our proposed spring bloom pre-  
 233 dictability mechanism (Fig. 3g), we find a strong inverse relationship between NPP and  
 234 earlier SIE in all sectors, which means anomalously low SIE leads to anomalously high  
 235 NPP, and vice versa. The relationship is strongest in the Weddell sector (Fig. 4a) where  
 236 November NPP anomalies have high correlation ( $r < -0.75$ ) with SIE anomalies up  
 237 to five lead months. The correlation is lower in the other sectors, but these sectors also  
 238 exhibit statistically significant negative correlation of November NPP anomalies with ear-  
 239 lier SIE anomalies up to five lead months. In all sectors aside from the Ross Sea, we also  
 240 find significant correlation between November NPP anomalies and SIE anomalies from  
 241 the previous year, corresponding to a winter-to-winter reemergence of SIE anomalies. When  
 242 examining surface irradiance as a predictor of NPP, we find a strong direct relationship  
 243 in all sectors, consistent with the expectation that increased light availability drives en-  
 244 hanced NPP. The positive IRR correlations with November NPP anomalies are signif-  
 245 icant at shorter lead times than the SIE correlations anomalies, but significant correla-  
 246 tion is maintained up to four months lead, as well as lead time beyond one year in all  
 247 regions except for the Ross Sea. This analysis suggests that if late winter and early spring  
 248 SIE and surface irradiance can be skillfully predicted, they should provide associated pre-  
 249 dictability for spring NPP, supporting the proposed predictability mechanism shown in  
 250 Fig. 3. The same correlation analysis was carried out for surface iron (Supporting Fig.  
 251 S6). Spring and summertime NPP is positively correlated with the previous winter's sur-  
 252 face iron concentrations in most sectors, but with correlation coefficients somewhat lower  
 253 than that of surface irradiance and SIE, particularly for a target month of November,  
 254 the month of maximum NPP predictability.

## 255 4 Discussion and Conclusions

256 Given the significant influence of NPP variations on marine ecosystems and emerg-  
 257 ing capabilities in biogeochemical modelling and data assimilation, there have been mul-  
 258 tiple recent studies assessing the predictability of NPP using ESMs on interannual time  
 259 scales (e.g., Frölicher et al., 2020; Séférian et al., 2014; Park et al., 2019; Taboada et al.,  
 260 2019; Chikamoto et al., 2015; Brune et al., 2022; Krumhardt et al., 2020). However, the  
 261 Southern Ocean seasonal ice zone, which differs from other regions due to the seasonal  
 262 advance and retreat of sea ice and associated drastic changes in the environmental con-  
 263 ditions, has received little attention so far. Here, we use a suite of PM experiments per-  
 264 formed with the GFDL-ESM2M model to assess the predictability of NPP and then ex-  
 265 amine how variations in sea ice retreat influence the predictability of NPP. We find that  
 266 NPP is predictable seven to ten years in advance in all regions except the Ross sector  
 267 (Fig. 1). NPP predictability tends to peak in November (eleven months from the Jan-  
 268 uary first initialization date), suggesting that skillful predictions of NPP on seasonal to  
 269 interannual time scales could be possible given accurate initial conditions. Moreover, since  
 270 SIE provides the dominant source of spring NPP predictability and recent studies have  
 271 shown skillful operational seasonal predictions of Antarctic SIE (e.g., Morioka et al., 2019;  
 272 Bushuk et al., 2021), skillful NPP predictions may be practically within reach.

273 In a Pan-Antarctic sense, and across most sectors, the progression of predictabil-  
 274 ity from SIE and MLD, to surface irradiance, and to NPP with a two to three months

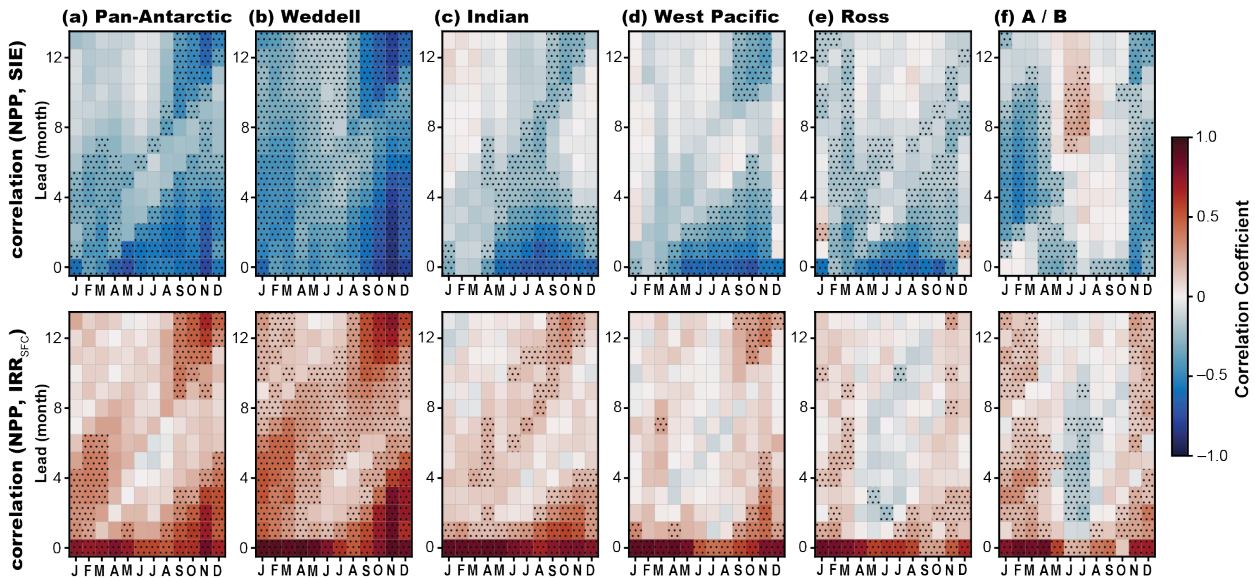


**Figure 4.** In the upper row, the Pearson correlation coefficient of net primary production (NPP) anomalies at target months January through December and sea ice extent (SIE) anomalies at 0-13 lead months in the (a) pan-Antarctic, (b) Weddell, (c) Indian, (d) West Pacific, (e) Ross, and (f) Amundsen/Bellingshausen sectors. In the lower row, the Pearson correlation coefficient of NPP anomalies at the same target months and surface irradiance (SFC\_IRR) anomalies at the same lead months. Correlation values are computed from the 300-year preindustrial control simulation. The dotting indicates Pearson correlation coefficient values significant at the 95% confidence level according to a  $t$ -test accounting for autocorrelation.

lag (Fig. 2 and 3a-f) supports our hypothesis that the spring bloom mechanism — relating the seasonal growth and melt of sea ice to both nutrient and light availability (Fig. 3g) — exerts control over the inherent predictability time scales of NPP and other spring bloom quantities. The correlation analysis (Fig. 4) shows a strong relationship between springtime NPP anomalies and earlier SIE and surface irradiance anomalies, supporting the PM predictability results. The sequence of these relationships aligns with what we causally expect given the spring bloom mechanism. Negative correlation between NPP and earlier SIE is expected since greater SIE inhibits phytoplankton growth by limiting light. Positive correlation between surface irradiance and NPP also agrees with the spring bloom mechanism since greater surface irradiance increases light availability, which promotes phytoplankton growth.

Nutrient availability could also play an important role in the predictability of NPP in some regions. The PM and correlation analyses (Fig. 2, and Supporting Fig. S5 and S6) indicate that predictability of wintertime nutrient concentrations are important for springtime NPP predictability in the A/B sector, and could play a role in the Weddell and Indian sectors. As prior work has indicated (Krumhardt et al., 2020), the major source of predictability is likely to come from whichever factor (light or nutrients) is most commonly limiting growth during the month of the spring bloom. While the model diagnostics necessary to assess this comprehensively are not available, the model's climatological seasonal cycle indicates that surface iron concentrations are not exhausted until January or February, supporting the possibility that November-time growth is not iron limited (Supporting Fig. S2). Further work, including assessing nutrient and light limitation within a PM framework, is required to fully assess the relative impact of these drivers

298 on NPP. The balance of these mechanisms has significant ramifications for the transla-  
299 tion of “potential predictability” into real world prediction skill, since observational con-  
300 straints for sea-ice extent and MLD are notably more abundant than those for nutrients.

301 There are clear regional differences in the predictability of NPP and other spring  
302 bloom quantities. The Weddell sector is consistently more predictable than all other re-  
303 gions, while the Ross sector is consistently the least predictable. The low predictabil-  
304 ity of NPP in the Ross sector is accompanied by low predictability in sea-ice (Fig. 2).  
305 The anomalously low sea ice predictability of the Ross Sea has also been identified in  
306 earlier work on seasonal predictions with other GFDL models (Bushuk et al., 2021), PM  
307 experiments performed with CCSM3 (Holland et al., 2013), and multi-model predictions  
308 submitted to SIPN-South (Massonnet et al., 2020). (Bushuk et al., 2021) speculated that  
309 the low Ross Sea sea ice predictability could be related to the strong meridional ice drift  
310 in this region, which implies that sea ice dynamics have a larger influence on the Ross  
311 sea ice edge position compared to other Antarctic regions. Since these ice dynamics are  
312 largely driven by unpredictable winds, this potentially makes the sea ice edge more dif-  
313 ficult to predict in this region. The spring bloom mechanism described above suggests  
314 that the inherent challenges in predicting Ross sea ice may translate to inherently low  
315 predictability of Ross NPP. However, the robustness of low Ross Sea predictability is still  
316 quite uncertain, as the multi-model PM study of Marchi et al. (2019) shows that there  
317 is substantial model diversity in Ross sea ice predictability, with some models exhibit-  
318 ing high predictability in this region.

319 While our PM framework allows us to examine the predictability of key variables  
320 in the GFDL-ESM2M model, it does have limitations. First, the ensemble members were  
321 initialized on a single date (January 1<sup>st</sup>) instead of choosing initialization dates through-  
322 out the year. The prediction skill of sea ice, for example, is highly dependent on the ini-  
323 tialization date of the dynamical prediction system (Bonan et al., 2019; Bushuk et al.,  
324 2021), which suggests that expanding our initialization dates could lead to different sea-  
325 sonal patterns of NPP predictability. Additionally, like many global models, GFDL-ESM2M  
326 exhibits multi-decadal variability in the subpolar Southern Ocean. In Supporting Text  
327 S2, we show that our results are not sensitive to the timing of initialization with respect  
328 to the phase of this variability. Second, our suite of PM experiments only uses a single  
329 model. While previous studies have shown that the GFDL-ESM2M model captures nat-  
330 ural variability and large-scale biogeochemical processes reasonably well (Dunne et al.,  
331 2012, 2013), there are unique features of the model that deviate from the real world and  
332 require us to interpret our results carefully. For example, it is questionable to what ex-  
333 tent current models are able to accurately capture the exact timing of the phytoplank-  
334 ton bloom in the Southern Ocean. While observations suggest that biomass starts in-  
335 creasing under sea ice prior to its retreat, peak biomass accumulation is expected in Novem-  
336 ber (Arteaga et al., 2020; Llort et al., 2015), which is consistent with the month of peak  
337 predictability in our experiments. Additionally, the biogeochemical model in ESM2M  
338 (TOPAZv2) lacks an explicit representation of zooplankton (Dunne et al., 2013), with  
339 phytoplankton loss via grazing represented as a function of phytoplankton abundance  
340 and temperature. Consequently, top-down controls, which could play an important role  
341 in the evolution of the spring bloom in the Southern Ocean (Rohr et al., 2017), are not  
342 fully represented.

343 In summary, we have assessed the predictability of NPP in the GFDL-ESM2M model  
344 using a suite of PM experiments. Given the important role of sea ice retreat in the spring  
345 bloom mechanism and recent work indicating that sea ice is predictable on seasonal-to-  
346 interannual time scales, we hypothesized that NPP and quantities relevant to the spring  
347 bloom should be predictable on similar time scales. Supporting our hypothesis, we find  
348 that November NPP is potentially predictable in all regions except the Ross sector for  
349 seven to ten years in advance, with highest predictability in the Weddell sector. By ex-  
350 amining the timing of the peak in predictability across quantities relevant to the spring

351 bloom, we find a temporal progression of maximum predictability from SIE and MLD,  
 352 to surface irradiance, and to NPP with a two to three months lag, aligning with the cli-  
 353 matological spring bloom mechanism. Lead-time correlations of SIE predicting NPP and  
 354 surface irradiance predicting NPP further support the progression of predictability. While  
 355 the robustness of these results still must be corroborated with other ESMs, the existence  
 356 of NPP predictability and the progression of predictability from SIE suggests that if we  
 357 can initialize a model accurately and skillfully predict SIE, then prediction skill should  
 358 exist for November NPP, potentially extending years in advance. Such skillful NPP pre-  
 359 dictions would be critical for predicting ecosystem changes and the biomass of living ma-  
 360 rine organisms, guiding fishery management, and informing marine conservation.

## 361 5 Open Research

362 Data and Jupyter notebooks to reproduce the figures in this manuscript are avail-  
 363 able on Zenodo (Buchovecky et al., 2023, <https://doi.org/10.5281/zenodo.8003803>).

## 364 Acknowledgments

365 This work was supported by the High Meadows Environmental Institute at Princeton  
 366 University and the NSF’s Southern Ocean Carbon and Climate Observations and Mod-  
 367 eling (SOCCOM) Project under the NSF Award PLR-1425989. F.A.H. was supported  
 368 by NASA Grant 80NSSC19K1115 and by the European Union (ERC, VERTEXSO, 101041743).  
 369 G.A.M was supported under SOCCOM and UKRI Grant MR/W013835/1. T.L.F was  
 370 supported by Swiss National Science Foundation (grant no. P00P2\_198897) and the Swiss  
 371 National Supercomputing Centre. N.L was supported by the European Union’s Hori-  
 372 zon 2020 research and innovation program under grant agreement no. 820989 (project  
 373 COMFORT) and no. 862923 (project AtlantECO). We are grateful to Yushi Morioka  
 374 and Jessica Luo for insightful comments on the manuscript, and Keith Rodgers for help  
 375 in setting up the model experiments.

## 376 References

- 377 Arrigo, K. R., van Dijken, G. L., & Bushinsky, S. (2008). Primary production in  
 378 the southern ocean, 1997–2006. *Journal of Geophysical Research: Oceans*,  
 379 *113*(C8). Retrieved from [https://agupubs.onlinelibrary.wiley.com/doi/](https://agupubs.onlinelibrary.wiley.com/doi/abs/10.1029/2007JC004551)  
 380 [abs/10.1029/2007JC004551](https://doi.org/10.1029/2007JC004551) doi: <https://doi.org/10.1029/2007JC004551>
- 381 Arteaga, L. A., Boss, E., Behrenfeld, M. J., Westberry, T. K., & Sarmiento, J. L.  
 382 (2020). Seasonal modulation of phytoplankton biomass in the southern ocean.  
 383 *Nature Communications*, *11*, 5364. doi: 10.1038/s41467-020-19157-2
- 384 Behrenfeld, M. J., Hu, Y., O’Malley, R. T., Boss, E. S., Hostetler, C. A., Siegel,  
 385 D. A., ... Scarino, A. J. (2017). Annual boom–bust cycles of polar phyto-  
 386 plankton biomass revealed by space-based lidar. *Nature Geoscience*, *10*(2),  
 387 118–122. doi: 10.1038/ngeo2861
- 388 Bonan, D. B., Bushuk, M., & Winton, M. (2019). A spring barrier for regional pre-  
 389 dictions of summer arctic sea ice. *Geophysical Research Letters*, *46*(11), 5937–  
 390 5947. doi: 10.1029/2019gl082947
- 391 Bretherton, C. S., Widmann, M., Dymnikov, V. P., Wallace, J. M., & Bladé,  
 392 I. (1999). The effective number of spatial degrees of freedom of a time-  
 393 varying field. *Journal of Climate*, *12*(7), 1990–2009. doi: 10.1175/  
 394 1520-0442(1999)012<1990:TENOSD>2.0.CO;2
- 395 Brooks, C. M., & Ainley, D. G. (2022). A summary of united states research and  
 396 monitoring in support of the ross sea region marine protected area. *Diversity*,  
 397 *14*(6). Retrieved from <https://www.mdpi.com/1424-2818/14/6/447> doi: 10  
 398 .3390/d14060447
- 399 Brune, S., Espejo, M. E. C., Nielsen, D. M., Li, H., Ilyina, T., & Baehr, J. (2022).

- 400 Oceanic Rossby waves drive inter-annual predictability of net primary produc-  
 401 tion in the central tropical Pacific. *Environmental Research Letters*, 17(1),  
 402 014030. doi: 10.1088/1748-9326/ac43e1
- 403 Buchovecky, B., MacGilchrist, G., Bushuk, M., Haumann, A., Frölicher, T., Le Grix,  
 404 N., & Dunne, J. (2023, June). *Potential Predictability of the Spring*  
 405 *Bloom in the Southern Ocean Sea Ice Zone: data and analysis scripts*. Zen-  
 406 odo. Retrieved from <https://doi.org/10.5281/zenodo.8003803> doi:  
 407 10.5281/zenodo.8003803
- 408 Bushuk, M., Winton, M., Haumann, F. A., Delworth, T., Lu, F., Zhang, Y., ...  
 409 Zeng, F. (2021). Seasonal prediction and predictability of regional antarctic  
 410 sea ice. *Journal of Climate*, 34(15), 6207–6233. doi: 10.1175/jcli-d-20-0965.1
- 411 Chassot, E., Bonhommeau, S., Dulvy, N. K., Mélin, F., Watson, R., Gascuel,  
 412 D., & Pape, O. L. (2010). Global marine primary production con-  
 413 strains fisheries catches. *Ecology Letters*, 13(4), 495–505. doi: 10.1111/  
 414 j.1461-0248.2010.01443.x
- 415 Chikamoto, M. O., Timmermann, A., Chikamoto, Y., Tokinaga, H., & Harada, N.  
 416 (2015). Mechanisms and predictability of multiyear ecosystem variability in  
 417 the North Pacific. *Global Biogeochemical Cycles*, 29(11), 2001–2019. doi:  
 418 10.1002/2015gb005096
- 419 Delworth, T. L., Broccoli, A. J., Rosati, A., Stouffer, R. J., Balaji, V., Beesley, J. A.,  
 420 ... Zhang, R. (2006). GFDL’s CM2 global coupled climate models. Part I:  
 421 Formulation and simulation characteristics. *Journal of Climate*, 19(5), 643–  
 422 674. doi: 10.1175/jcli3629.1
- 423 Deppeler, S. L., & Davidson, A. T. (2017). Southern ocean phytoplankton in a  
 424 changing climate. *Frontiers in Marine Science*, 4, 40. doi: 10.3389/fmars.2017  
 425 .00040
- 426 Douglas, C. C., Briggs, N., Brown, P., MacGilchrist, G., & Naveira Garabato, A.  
 427 (2023). Exploring the relationship between sea-ice and primary production in  
 428 the weddell gyre using satellite and argo-float data.
- 429 Dunne, J. P., John, J. G., Adcroft, A. J., Griffies, S. M., Hallberg, R. W., Shevli-  
 430 akova, E., ... Zadeh, N. (2012). GFDL’s ESM2 global coupled Cli-  
 431 mate–Carbon earth system models. Part I: Physical formulation and base-  
 432 line simulation characteristics. *Journal of Climate*, 25(19), 6646–6665. doi:  
 433 10.1175/jcli-d-11-00560.1
- 434 Dunne, J. P., John, J. G., Shevliakova, E., Stouffer, R. J., Krasting, J. P., Maly-  
 435 shev, S. L., ... Zadeh, N. (2013). GFDL’s ESM2 global coupled Cli-  
 436 mate–Carbon earth system models. Part II: Carbon system formulation and  
 437 baseline simulation characteristics. *Journal of Climate*, 26(7), 2247–2267. doi:  
 438 10.1175/jcli-d-12-00150.1
- 439 Friedland, K. D., Stock, C., Drinkwater, K. F., Link, J. S., Leaf, R. T., Shank,  
 440 B. V., ... Fogarty, M. J. (2012). Pathways between primary production and  
 441 fisheries yields of large marine ecosystems. *PLoS ONE*, 7(1), e28945. doi:  
 442 10.1371/journal.pone.0028945
- 443 Frölicher, T. L., Ramseyer, L., Raible, C. C., Rodgers, K. B., & Dunne, J. (2020).  
 444 Potential predictability of marine ecosystem drivers. *Biogeosciences (Online)*,  
 445 17(7), 2061–2083. doi: 10.5194/bg-17-2061-2020
- 446 Griffies, S. M., Gnanadesikan, A., Dixon, K. W., Dunne, J. P., Gerdes, R., Harrison,  
 447 M. J., ... Zhang, R. (2005). Formulation of an ocean model for global climate  
 448 simulations. *Ocean Science*, 1(1), 45–79. doi: 10.5194/os-1-45-2005
- 449 Ham, Y.-G., Joo, Y.-S., & Park, J.-Y. (2021). Mechanism of skillful seasonal surface  
 450 chlorophyll prediction over the southern Pacific using a global earth system  
 451 model. *Climate Dynamics*, 56(1-2), 45–64. doi: 10.1007/s00382-020-05403-2
- 452 Holland, M. M., Blanchard-Wrigglesworth, E., Kay, J., & Vavrus, S. (2013).  
 453 Initial-value predictability of Antarctic sea ice in the Community Climate  
 454 System Model 3. *Geophysical Research Letters*, 40(10), 2121–2124. doi:

- 455 10.1002/grl.50410
- 456 Krumhardt, K. M., Lovenduski, N. S., Long, M. C., Luo, J. Y., Lindsay, K., Yeager,  
457 S., & Harrison, C. (2020). Potential predictability of net primary production in  
458 the ocean. *Global Biogeochemical Cycles*, *34*(6). doi: 10.1029/2020gb006531
- 459 Llort, J., Lévy, M., Sallée, J.-B., & Tagliabue, A. (2015, 04). Onset, intensifica-  
460 tion, and decline of phytoplankton blooms in the Southern Ocean. *ICES Jour-  
461 nal of Marine Science*, *72*(6), 1971-1984. Retrieved from [https://doi.org/10.  
462 .1093/icesjms/fsv053](https://doi.org/10.1093/icesjms/fsv053) doi: 10.1093/icesjms/fsv053
- 463 Marchi, S., Fichefet, T., Goosse, H., Zunz, V., Tietsche, S., Day, J. J., & Hawkins,  
464 E. (2019). Reemergence of Antarctic sea ice predictability and its link to deep  
465 ocean mixing in global climate models. *Climate Dynamics*, *52*(5-6), 2775–2797.  
466 doi: 10.1007/s00382-018-4292-2
- 467 Massonnet, F., Reid, P., Lieser, J. L., Bitz, C. M., Fyfe, J., & Hobbs, W. (2020).  
468 *Assessment of summer 2019-2020 sea-ice forecasts for the southern ocean*. doi:  
469 <https://fmassonn.github.io/sipnsouth.github.io/>
- 470 Moore, J. K., & Abbott, M. R. (2000). Phytoplankton chlorophyll distribu-  
471 tions and primary production in the southern ocean. *Journal of Geophys-  
472 ical Research: Oceans*, *105*(C12), 28709-28722. Retrieved from [https://  
473 agupubs.onlinelibrary.wiley.com/doi/abs/10.1029/1999JC000043](https://agupubs.onlinelibrary.wiley.com/doi/abs/10.1029/1999JC000043) doi:  
474 <https://doi.org/10.1029/1999JC000043>
- 475 Moreau, S., Boyd, P. W., & Strutton, P. G. (2020). Remote assessment of the fate  
476 of phytoplankton in the Southern Ocean sea-ice zone. *Nature Communications*,  
477 *11*(1), 3108. doi: 10.1038/s41467-020-16931-0
- 478 Morioka, Y., Doi, T., Iovino, D., Masina, S., & Behera, S. K. (2019, February). Role  
479 of sea-ice initialization in climate predictability over the Weddell Sea. *Scientific  
480 Reports*, *9*(1), 2457. doi: 10.1038/s41598-019-39421-w
- 481 Park, J.-Y., Stock, C. A., Dunne, J. P., Yang, X., & Rosati, A. (2019). Seasonal to  
482 multiannual marine ecosystem prediction with a global Earth system model.  
483 *Science (New York, N.Y.)*, *365*(6450), 284–288. doi: 10.1126/science.aav6634
- 484 Pohlmann, H., Botzet, M., Latif, M., Roesch, A., Wild, M., & Tschuck, P. (2004).  
485 Estimating the decadal predictability of a coupled AOGCM. *Journal of Cli-  
486 mate*, *17*(22), 4463–4472. doi: 10.1175/3209.1
- 487 Rohr, T., Long, M. C., Kavanaugh, M. T., Lindsay, K., & Doney, S. C. (2017).  
488 Variability in the mechanisms controlling southern ocean phytoplankton bloom  
489 phenology in an ocean model and satellite observations. *Global Biogeochemical  
490 Cycles*, *31*(5), 922–940.
- 491 Séférian, R., Bopp, L., Gehlen, M., Swingedouw, D., Mignot, J., Guilyardi, E., &  
492 Servonnat, J. (2014). Multiyear predictability of tropical marine productivity.  
493 *Proceedings of the National Academy of Sciences*, *111*(32), 11646–11651. doi:  
494 10.1073/pnas.1315855111
- 495 Stock, C. A., Dunne, J. P., & John, J. G. (2014). Drivers of trophic amplification of  
496 ocean productivity trends in a changing climate. *Biogeosciences*, *11*(24), 7125–  
497 7135. doi: 10.5194/bg-11-7125-2014
- 498 Stock, C. A., John, J. G., Rykaczewski, R. R., Asch, R. G., Cheung, W. W. L.,  
499 Dunne, J. P., ... Watson, R. A. (2017). Reconciling fisheries catch and ocean  
500 productivity. *Proceedings of the National Academy of Sciences*, *114*(8), E1441–  
501 E1449. doi: 10.1073/pnas.1610238114
- 502 Taboada, F. G., Barton, A. D., Stock, C. A., Dunne, J., & John, J. G. (2019).  
503 Seasonal to interannual predictability of oceanic net primary production in-  
504 ferred from satellite observations. *Progress in Oceanography*, *170*, 28–39. doi:  
505 10.1016/j.pocean.2018.10.010
- 506 Tagliabue, A., Kwiatkowski, L., Bopp, L., Butenschön, M., Cheung, W., Lengaigne,  
507 M., & Vialard, J. (2021). Persistent uncertainties in ocean net primary  
508 production climate change projections at regional scales raise challenges for  
509 assessing impacts on ecosystem services. *Frontiers in Climate*, *3*, 738224. doi:

- 510 10.3389/fclim.2021.738224  
511 Taylor, M. H., Losch, M., & Bracher, A. (2013). On the drivers of phytoplankton  
512 blooms in the Antarctic marginal ice zone: A modeling approach. *Journal of*  
513 *Geophysical Research: Oceans*, *118*(1), 63–75. doi: 10.1029/2012jc008418  
514 Uchida, T., Balwada, D., Abernathy, R., Prend, C. J., Boss, E., & Gille, S. T.  
515 (2019). Southern ocean phytoplankton blooms observed by biogeochemical  
516 floats. *Journal of Geophysical Research: Oceans*, *124*(11), 7328–7343. doi:  
517 10.1029/2019jc015355  
518 Winton, M. (1999). A reformulated three-layer sea ice model. *Journal of Atmo-*  
519 *spheric and Oceanic Technology*.